Journal of the Korean Physical Society, Vol. 56, No. 3, March 2010, pp. 963∼968

Torus Doublings in Symmetrically Coupled Period-doubling Systems

Sang-Yoon Kim* and Woochang Lim†
Department of Physics, Kangwon National University, Chunchon 200-701

Youngtae Kim‡
Department of Physics, Ajou University, Suwon 442-749

(Received 15 September 2009, in final form 13 January 2010)

As a representative model for Poincaré maps of coupled period-doubling oscillators, we consider two symmetrically coupled Hénon maps. Each invertible Hénon map has a constant Jacobian b ($0 < b < 1$) controlling the "degree" of dissipation. For the singular case of infinite dissipation ($b = 0$), it reduces to the non-invertible logistic map. Instead of period-doubling bifurcations, anti-phase periodic orbits (with a time shift of half a period) lose their stability via Hopf bifurcations, and then smooth tori, encircling the anti-phase mother orbits, appear. We study the fate of these tori by varying b. For large b, doubled tori are found to appear via torus doubling bifurcations. This is in contrast to the case of coupled logistic maps without torus doublings. With decreasing b, mechanisms for disappearance of torus doublings are investigated, and doubled tori are found to be replaced with simple tori, periodic attractors, or chaotic attractors for small b. These torus doublings are also observed in two symmetrically coupled pendula that individually display a period-doubling transition to chaos.

PACS numbers: 05.45.Ac
Keywords: Nonlinear dynamics, Bifurcation, Period-doubling system, Coupled system, torus doubling
DOI: 10.3938/jkps.56.963

I. INTRODUCTION

Much attention has been paid to transitions from torus to chaos in dissipative dynamical systems [1]. A well-known route to chaos is a quasiperiodic transition to chaos in systems with two competing frequencies. This scenario was intensively investigated in the circle map [2,3], and universal critical scaling behaviors were found. Another interesting route to chaos is a torus-doubling transition to chaos, which is a higher-dimensional phenomenon, requiring at least a four-dimensional flow (or a three-dimensional invertible Poincaré map) [4]. This scenario was first studied by Kaneko [4]. He combined the logistic map (exhibiting period doublings) [5] and the circle map (showing quasiperiodicity) and found torus doublings. However, unlike the period-doubling transition to chaos, only a finite number of torus doublings are observed before chaos occurs. Similar results were obtained in the three-dimensional dissipative map to model the effect of periodic forcing on period-doubling systems [6]. This type of torus-doubling transition to chaos was also found in continuous-time systems governed by differential equations, such as the Navier-Stokes equation [7] and the Ginzburg-Landau equation [8]. Furthermore, this interesting phenomenon of torus doublings was observed in experiments on Rayleigh-Bénard convection [9, 10], the convection in molten gallium [11], the electrochemical reaction [12], the ferroelectric KDP crystal [13], and the metal-ferroelectric film-semiconductor capacitor [14].

In this paper, we are interested in torus doublings occurring in symmetrically coupled period-doubling systems. Our coupled system (composed of two period-doubling subsystems) is in contrast to the previously-studied combined system consisting of a period-doubling subsystem and a quasiperiodic subsystem [4,6]. As a representative model for Poincaré maps of coupled period-doubling oscillators, we consider two symmetrically coupled Hénon maps [15]. Each invertible Hénon map has a constant Jacobian b ($0 < b < 1$) that controls the degree of dissipation. In these two coupled Hénon maps, a symmetric anti-phase periodic orbit with a time shift of half a period is born via a period-doubling bifurcation of the symmetric in-phase periodic orbit. Instead of period-doubling bifurcations, these anti-phase orbits become unstable via Hopf bifurcations [16–18]. Thus, smooth tori, surrounding the anti-phase mother orbits, appear. In Sec. II., we study the fate of these tori by varying the dissipation parameter b. For large b, dou-

*E-mail: sykim@kangwon.ac.kr
†E-mail: wclim@kangwon.ac.kr
‡Corresponding Author; E-mail: ytkim@ajou.ac.kr

bled tori are found to appear via torus-doubling bifurcations, in contrast to the case of coupled logistic maps without torus doublings. With decreasing b, we investigate the mechanisms for disappearance of torus doublings and find that doubled tori are replaced with simple tori, periodic attractors, or chaotic attractors for small b. These torus doublings are also observed in two symmetrically coupled pendula, which individually exhibit period-doubling transition to chaos. Finally, in Sec. III., we give a summary.

II. TORUS DOUBLINGS IN SYMMETRICALLY COUPLED PERIOD-DOUBLING OSCILLATORS

As a representative model for Poincaré maps of coupled period-doubling oscillators, we consider two symmetrically coupled Hénon maps:

$$T: \begin{cases} x_1(n+1) = -y_1(n) + f(x_1(n)) + \varepsilon\,[x_2(n) - x_1(n)], \\ y_1(n+1) = b x_1(n), \\ x_2(n+1) = -y_2(n) + f(x_2(n)) + \varepsilon\,[x_1(n) - x_2(n)], \\ y_2(n+1) = b x_2(n), \end{cases} \tag{1}$$

where $f(x) = 1 - ax^2$, $z_i(n)$ $[\equiv (x_i(n), y_i(n))]$ is a state variable of the ith $(i = 1, 2)$ element at a discrete time n, and ε is a coupling parameter. Each invertible Hénon map has a constant Jacobian b $(0 < b < 1)$ that controls the degree of dissipation. For the singular case of infinite dissipation $(b = 0)$, it reduces to a non-invertible one-dimensional logistic map [5]. In a single Hénon map, a period-doubling transition to chaos occurs as the nonlinearity parameter a passes a threshold value a^*. We also note that the coupled map T has an exchange symmetry S such that

$$S\,T\,S(z_1, z_2) = T(z_1, z_2);\ S(z_1, z_2) = (z_2, z_1). \tag{2}$$

If an orbit is invariant under S, it is called a symmetric orbit; otherwise, it is called an asymmetric orbit.

For the uncoupled case of $\varepsilon = 0$, the coupled map of Eq. (1) breaks up into two uncoupled Hénon maps. If they both have orbits with period q, then the composite system has q different orbits distinguished by the phase shift s $(= 0, 1, \ldots, q-1)$. The case of $s = 0$ corresponds to that of an in-phase orbit, while the other cases of $s \neq 0$ correspond to those of out-of-phase orbits. If $s = q/2$, then an anti-phase (180° out-of-phase) orbit with a time shift of half a period exists; otherwise $(s \neq q/2)$, non-antiphase orbits appear. The in-phase and the anti-phase periodic orbits are symmetric with respect to the exchange symmetry S while other periodic orbits are asymmetric. Two asymmetric period-q orbits with phase shifts s and $q - s$ are conjugate because one orbit is transformed into the other one under an exchange of coordinates S. All periodic orbits associated with a period-doubling cascade of the Hénon map persist when the coupling is introduced, at least while its value is small enough. Hereafter, we classify such periodic orbits in terms of their periods and phase shifts (q, s).

The stability of an orbit with period q in the two coupled Hénon maps of Eq. (1) is determined from the Jacobian matrix J of T^q, which is the q-product of the Jacobian matrix DT of T along the orbit:

$$\begin{aligned} J &= \prod_{n=1}^{q} DT(x_1(n), y_1(n), x_2(n), y_2(n)) \\ &= \prod_{n=1}^{q} \begin{pmatrix} f'(x_1(n)) - \varepsilon & -1 & \varepsilon & 0 \\ b & 0 & 0 & 0 \\ \varepsilon & 0 & f'(x_2(n)) - \varepsilon & -1 \\ 0 & 0 & b & 0 \end{pmatrix}, \end{aligned} \tag{3}$$

where $f'(x) = df(x)/dx$. The eigenvalues of J (λ_1, λ_2, λ_3, and λ_4) are called the stability multipliers of the orbit. An orbit is stable only when the moduli of all multipliers are less than unity (*i.e.*, $|\lambda_i| < 1$ $(i = 1, 2, 3, 4)$; all of them lie inside a unit circle in the complex plane). When a multiplier passes the unit circle at $\lambda = 1$ (-1), the orbit becomes unstable via a saddle-node or pitchfork (period-doubling) bifurcation. On the other hand, as a multiplier crosses the unit circle except $\lambda = \pm 1$ (*i.e.*, λ becomes a complex number whose magnitude is larger than unity), the orbit loses its stability through a Hopf bifurcation. The type of attractors in the two coupled maps is determined in terms of their Lyapunov exponents (σ_1, σ_2, σ_3, and σ_4; $\sigma_1 \geq \sigma_2 \geq \sigma_3 \geq \sigma_4$). By iterating the Jacobian matrix of DT along a trajectory, such Lyapunov exponents are obtained through the Gram-Schmidt reorthonormalization procedure [19]. When the largest Lyapunov exponent σ_1 is negative (zero), the attractor is a periodic (quasiperiodic) one. On the other hand, it is a chaotic one when σ_1 is positive. Furthermore, a hyperchaotic attractor with more than one positive Lyapunov exponents may appear.

We first consider the case of $b = 0.5$. Figure 1(a) shows plots of the first two Lyapunov exponents (σ_1 and σ_2) of an attractor versus a for $\varepsilon = -0.305$. The corresponding bifurcation diagram (*i.e.*, plot of x_1 versus a) is also given in Fig. 1(b). An anti-phase period-4 attractor becomes unstable for $a = 2.018\,012$ via a Hopf bifurcation when a pair of complex-conjugate stability multipliers passes the unit circle (*i.e.*, $\sigma_1 = \sigma_2 = 0$). Thus, a smooth torus with $\sigma_1 = 0$ and $\sigma_2 < 0$ appears, as shown in Fig. 1(c) for $a = 2.04$. As a is increased, the second Lyapunov exponent σ_2 begins to increase, and it becomes zero for $a = a_n$ $(\simeq 2.045)$ [see the point indicated by **n** in Fig. 1(a)]. Then, through a normal torus-doubling bifurcation [20], a doubled torus with $\sigma_1 = 0$ and $\sigma_2 < 0$ appears, as shown in Fig. 1(d) for $a = 2.05$. As a is increased a little, the second Lyapunov exponent of the doubled torus becomes zero again for $a = a_r$ $(\simeq 2.055)$ [see the point indicated by **r** in Fig. 1(a)]. Then,

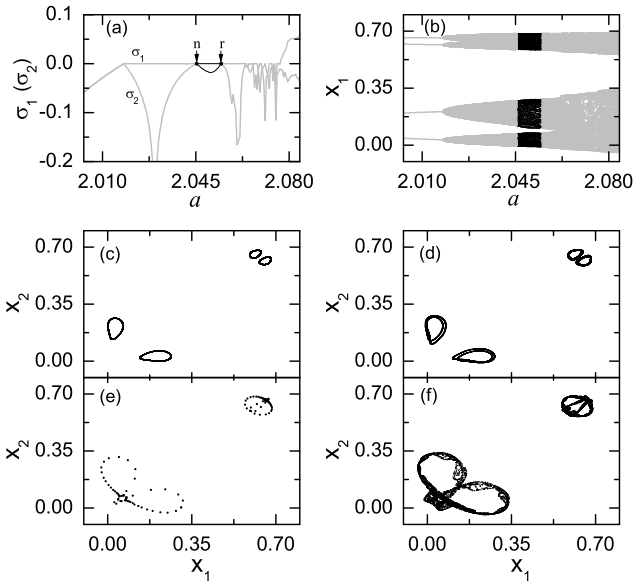

Fig. 1. We set $b = 0.5$ and $\epsilon = -0.305$ in (a)-(f). (a) Plots of σ_1 and σ_2 versus a. The Lyapunov exponents of the doubled torus are represented by black curves while the Lyapunov exponents of other attractors are denoted by gray curves. Normal and reverse torus-doubling bifurcations occur for $a = a_n$ and a_r indicated by **n** and **r**, respectively. (b) Plot of x_1 versus a. The bifurcation diagram of the doubled torus (other attractors) is shown in black (gray). (c) Smooth torus with $\sigma_1 = 0$ and $\sigma_2 = -0.024$ for $a = 2.04$. (d) Doubled torus with $\sigma_1 = 0$ and $\sigma_2 = -0.017$ for $a = 2.05$. (e) Period-108 attractor with $\sigma_1 = -0.007$ and $\sigma_1 = -0.01$ for $a = 2.07$. (f) Chaotic attractor with $\sigma_1 = 0.049$ and $\sigma_2 = -0.031$ for $a = 2.08$.

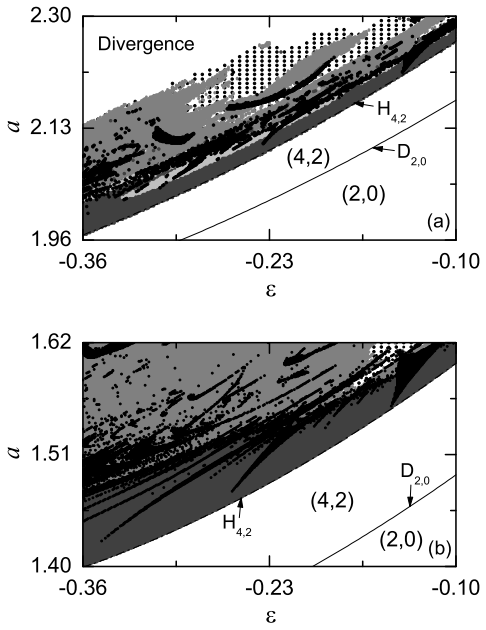

Fig. 2. (a) State diagram for $b = 0.5$ near a Hopf bifurcation curve $H_{4,2}$ of the anti-phase period-4 orbit. The anti-phase orbit of type (4,2) appears via a period-doubling bifurcation of the in-phase orbit of type (2,0) when passing the curve $D_{2,0}$. Mode locking, quasiperiodicity, chaos, hyperchaos, and divergence occur in the black, dark-gray, gray, dotted, white regions, respectively. Note that doubled tori exist in the light-gray region. (b) State diagram for $b = 0.2$. No doubled tori exist.

a reverse torus-doubling bifurcation occurs, and a simple torus [like that shown in Fig. 1(c)] appears again. Thus, a doubled torus exists in the interval (a_n, a_r). The Lyapunov exponents of the doubled torus are denoted by the black curves in Fig. 1(a) while the Lyapunov exponents of other attractors are represented by gray curves. Similarly, the bifurcation diagram of the doubled torus (other attracors) is shown in black (gray) in Fig. 1(b). As a is further increased from a_r and passes a threshold value a^* ($\simeq 2.077$), a transition to chaos, accompanied by mode lockings, occurs. As examples, see the periodic and the chaotic attractors shown in Figs. 1(e)-1(f) for $a = 2.07$ and 2.08, respectively.

We are interested in the effect of dissipation on torus doublings. Figure 2(a) shows the state diagram near a Hopf bifurcation curve of the anti-phase period-4 orbit for $b = 0.5$. The anti-phase orbit of type (4,2) appears via a period-doubling bifurcation of the in-phase orbit of type (2,0) when passing the solid curve $D_{2,0}$. The stability regions of the in-phase and the anti-phase orbits are labeled as types (2,0) and (4,2), respectively. The anti-phase orbit loses its stability via a Hopf bifurcation at the dash-dotted curve $H_{4,2}$. Consequently, mode locking (shown in black) and quasiperiodicity (shown in dark gray) occur. We note that doubled tori, born via torus-doubling bifurcations, exist in the light-gray region. This is in contrast to the case of coupled logistic maps without torus doublings. [If a torus doubling occurs in the two-dimensional phase plane of the coupled logistic maps, then the closed curve (corresponding to a cross section of a torus) must intersect itself, which results in a violation of uniqueness of an orbit.] With further increases in a, chaos, hyperchaos, and divergence occur in the gray, dotted, and white regions, respectively. However, as the dissipation parameter b is decreased, the region where doubled tori exist shrinks, and eventually it seems to disappear when b passes a threshold $b^*(\sim 0.4)$. As an example, see the state diagram for $b = 0.2$ in Fig. 2(b). For this case, no regions of doubled tori are found, in contrast to the case of $b = 0.5$ in Fig. 2(a).

We investigate the mechanisms for disappearance of torus doublings by decreasing the dissipation parameter b and find three cases. As b is decreased from $b = 0.5$ for $\varepsilon = -0.305$, the normal and the reverse torus-doubling points (indicated by **n** and **r**) in Fig. 1(a) approach; hence, the parameter interval where doubled tori exist decreases. Eventually, when passing a threshold value, the two torus-doubling points merge; then, the σ_2 curve becomes detached from the σ_1 curve without touching, as shown in Fig. 3(a) for $b = 0.4$. Thus, no torus doublings

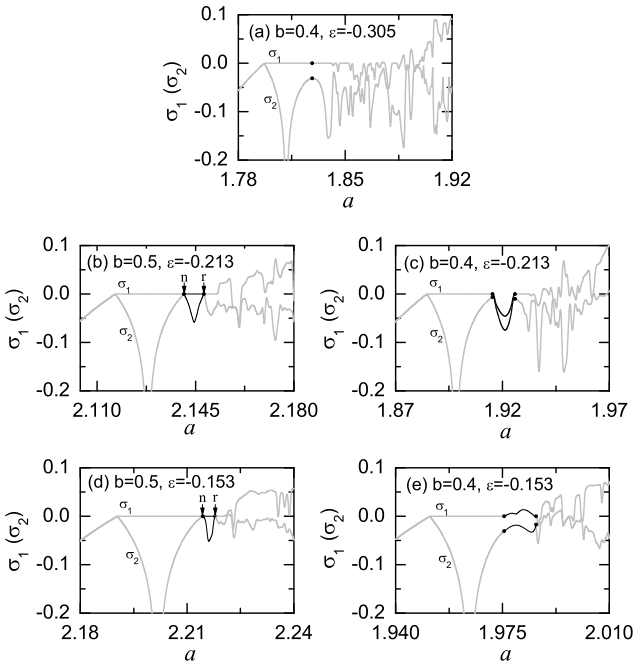

Fig. 3. Lyapunov-exponent diagrams of σ_1 and σ_2 for (a) $b = 0.5$ and $\varepsilon = -0.305$, (b) $b = 0.5$ and $\varepsilon = -0.213$, (c) $b = 0.4$ and $\varepsilon = -0.213$, (d) $b = 0.5$ and $\varepsilon = -0.153$, and (e) $b = 0.4$ and $\varepsilon = -0.153$.

occur for $b = 0.4$, in contrast to the case of $b = 0.5$. This first case shows disappearance of torus doublings through replacement of doubled tori with simple tori. A second case for the disappearance of torus doublings occurs through "invasion" of mode lockings with $\sigma_1 < 0$. Figures 3(b) and 3(c) show the Lyapunov exponent diagrams of σ_1 and σ_2 for $b = 0.5$ and 0.4 in the case of $\varepsilon = -0.213$, respectively. For $b = 0.5$, doubled tori exist in a parameter interval denoted by a black curve (with endpoints indicated by **n** and **r**). However, such a doubled-torus interval is replaced by a mode-locked one for $\sigma_1 < 0$ and $b = 0.4$. A third case for the disappearance of torus doublings occurs via "invasion" of chaotic attractors for $\sigma_1 > 0$. The Lyapunov exponent diagrams of σ_1 and σ_2 are shown in Figs. 3(d) and 3(e) for $b = 0.5$ and 0.4 in the case of $\varepsilon = -0.153$, respectively. The doubled-torus interval for $b = 0.5$ is replaced with a chaotic one for $\sigma_1 > 0$ and $b = 0.4$.

Finally, we confirm the above results (obtained in the abstract system of coupled Hénon maps) in the Poincaré map of two symmetrically coupled pendulums [21]:

$$\dot{x_1} = y_1, \;\; \dot{y_1} = f(x_1, y_1, t) + \varepsilon(x_2 - x_1), \tag{4a}$$

$$\dot{x_2} = y_2, \;\; \dot{y_2} = f(x_2, y_2, t) + \varepsilon(x_1 - x_2), \tag{4b}$$

where

$$f(x, \dot{x}, t) = -2\pi\beta\Omega\dot{x} - 2\pi(\Omega^2 - A\cos 2\pi t)\sin 2\pi x, \tag{5}$$

and ε is the coupling parameter. For each parametrically forced pendulum [22], x is a normalized angle with range $x \in [-\frac{1}{2}, \frac{1}{2})$, β is a normalized damping parameter, Ω is the normalized natural frequency of the unforced pendulum, and A is the normalized driving amplitude of the vertical oscillation of the suspension point. Here, we set $\beta = 0.1$ and $\Omega = 1.0$. As the amplitude A of the vertical oscillation is increased, the lowest stationary point with $x = 0$ loses its stability via a (symmetry-breaking) pitchfork bifurcation; then, an infinite sequence of period-doubling bifurcations, leading to chaos, follows, as in the case of the logistic map [22].

Poincaré maps of Eq. (4) can be computed by stroboscopically sampling the points $\mathbf{z}(n)$ [$\equiv (z_1(n), z_2(n))$; $z_i = (x_i, y_i)$, $i = 1, 2$] at the discrete time n, where $n = 1, 2, 3, \ldots$. We call the transformation $\mathbf{z}(n) \to \mathbf{z}(n+1)$ the Poincaré map of the two coupled pendula. This four-dimensional (4D) Poincaré map P has an exchange symmetry such that

$$SPS(z_1, z_2) = P(z_1, z_2); \; S(z_1, z_2) = (z_2, z_1). \tag{6}$$

Periodic orbits in P may be classified in terms of their periods and phase shifts (q, p), as in the case of coupled Hénon maps. In-phase ($s = 0$) and anti-phase orbits ($s = q/2$) are symmetric with respect to the exchange symmetry S while other periodic orbits are asymmetric.

The linear stability of a q-periodic orbit such that $P^q(\mathbf{z}(0)) = \mathbf{z}(0)$ is determined from the linearized map $DP^q(\mathbf{z}(0))$ of P^q at an orbit point $\mathbf{z}(\mathbf{0})$, where P^q means the q-times iterated map. With the Floquet theory [23], DP^q can be obtained by integrating the linearized differential equations for small perturbations. Let $\mathbf{z}^*(t) = \mathbf{z}^*(t+q)$ be a solution lying on the closed orbit corresponding to the q-periodic orbit. In order to determine the stability of the closed orbit, we consider an infinitesimal perturbation $\delta\mathbf{z}$ [$= (\delta x_1, \delta y_1, \delta x_2, \delta y_2)$] to the closed orbit. Linearizing Eq. (4) about the closed orbit, we obtain

$$\begin{pmatrix} \delta\dot{x}_1 \\ \delta\dot{y}_1 \\ \delta\dot{x}_2 \\ \delta\dot{y}_2 \end{pmatrix} = J(t) \begin{pmatrix} \delta x_1 \\ \delta y_1 \\ \delta x_2 \\ \delta y_2 \end{pmatrix}, \tag{7}$$

where the Jacobian matrix J is given by

$$J(t) = \begin{pmatrix} 0 & 1 & 0 & 0 \\ J_{21} & J_{22} & J_{23} & 0 \\ 0 & 0 & 0 & 1 \\ J_{41} & 0 & J_{43} & J_{44} \end{pmatrix}; \tag{8a}$$

$$J_{21} = -4\pi^2(\Omega^2 - A\cos 2\pi t)\cos 2\pi x_1^* - \varepsilon, \tag{8b}$$

$$J_{22} = -2\pi\beta\Omega, \; J_{23} = \varepsilon, \tag{8c}$$

$$J_{41} = \varepsilon, \; J_{43} = -4\pi^2(\Omega^2 - A\cos 2\pi t)\cos 2\pi x_2^* - \varepsilon, \tag{8d}$$

$$J_{44} = -2\pi\beta\Omega. \tag{8e}$$

Note that J is a 4×4 q-periodic matrix. Let $W(t) = (w^1(t), w^2(t), w^3(t), w^4(t))$ be a fundamental solution matrix with $W(0) = I$. Here, $w^1(t)$, $w^2(t)$, $w^3(t)$, and

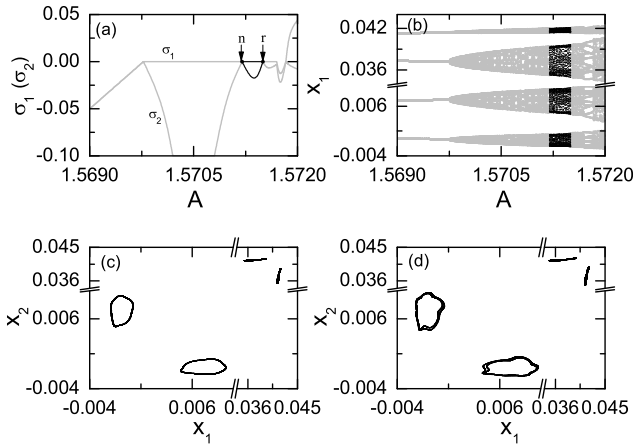

Fig. 4. Torus doublings in the Poincaré map of symmetrically coupled pendulums for $\beta = 0.1$, $\Omega = 1.0$, and $\varepsilon = 0.6$. (a) Plots of σ_1 and σ_2 versus A. Normal and reverse torus-doubling bifurcations occur for $A = A_n$ and A_r indicated by **n** and **r**, respectively. The Lyapunov exponents of the doubled tori are represented by black curves. (b) Plot of x_1 versus A. The doubled torus is shown in black. (c) Smooth torus with $\sigma_1 = 0$ and $\sigma_2 = -0.037$ for $A = 1.571$. (d) Doubled torus with $\sigma_1 = 0$ and $\sigma_2 = -0.016$ for $A = 1.5714$.

$w^4(t)$ are four independent solutions expressed in column vector forms, and I is the 4×4 unit matrix. Then, a general solution of the q-periodic system has the form

$$\begin{pmatrix} \delta x_1(t) \\ \delta y_1(t) \\ \delta x_2(t) \\ \delta y_2(t) \end{pmatrix} = W(t) \begin{pmatrix} \delta x_1(0) \\ \delta y_1(0) \\ \delta x_2(0) \\ \delta y_2(0) \end{pmatrix}. \tag{9}$$

Substitution of Eq. (9) into Eq. (7) leads to an initial-value problem to determine $W(t)$:

$$\dot{W}(t) = J(t)W(t), \;\; W(0) = I. \tag{10}$$

It is clear from Eq. (9) that $W(q)$ is just the linearized map DP^q. Hence, DP^q may be calculated through integration of Eq. (10) over the period q. A periodic orbit is stable only when the moduli of all four stability multipliers (*i.e.*, the eigenvalues of DP^q) are less than unity. (Detailed explanations of the bifurcations through which a periodic orbit loses its stability are given in the above case of coupled Hénon maps.) The type of attractor in the Poincaré map P is determined in terms of its Lyapunov exponents (σ_1, σ_2, σ_3, and σ_4; $\sigma_1 \geq \sigma_2 \geq \sigma_3 \geq \sigma_4$). Through an iteration of the linearized Poincare map DP for an initial perturbation $\delta\mathbf{z}$ along the orbit, such Lyapunov exponents are obtained through the Gram-Schmidt reorthonormalization procedure [19]. When the largest Lyapunov exponent σ_1 is negative, zero, and positive, the attractor is a periodic, quasiperiodic, and chaotic, respectively.

Figure 4(a) shows Lyapunov-exponent diagrams of σ_1 and σ_2 of an attractor versus A in the Poincaré map P of symmetrically coupled pendula for $\varepsilon = 0.6$. The corresponding bifurcation diagram (*i.e.*, plot of x_1 versus A) is shown in Fig. 4(b). An anti-phase period-4 attractor becomes unstable at the Hopf bifurcation point of $A = 1.569\,772$, where $\sigma_1 = \sigma_2 = 0$. Then, a smooth tori with $\sigma_1 = 0$ and $\sigma_2 < 0$ appears, as shown in Fig. 4(c) for $A = 1.571$. As A is increased, the second Lyapunov exponent σ_2 begins to increase and becomes zero for $A = A_n$ ($\simeq 1.5712$) [see the point indicated by **n** in Fig. 4(a)]. Then, a doubled torus with $\sigma_1 = 0$ and $\sigma_2 < 0$ appears via a normal torus-doubling bifurcation, as shown in Fig. 4(d) for $A = 1.5714$. As A is increased a little, the second Lyapunov exponent of the doubled torus becomes zero again for $A = A_r$ ($\simeq$1.5715) [see the point indicated by **r** in Fig. 4(a)]. Then, a reverse torus-doubling bifurcation occurs, and a simple torus [like that shown in Fig. 4(c)] reappears. Thus, a doubled torus exists in the interval (A_n, A_r), as in the case of coupled Hénon maps.

III. SUMMARY

We have investigated torus doublings in symmetrically coupled period-doubling systems. As a representative model for Poincaré maps of coupled period-doubling oscillators, we consider two symmetrically coupled Hénon maps. Instead of period doubling bifurcations occurring in each Hénon map, anti-phase periodic orbits lose their stability via Hopf bifurcations. Consequently, smooth tori, encircling the anti-phase orbits, appear. The fate of these tori has been investigated by varying the dissipation parameter b. For large b doubled tori are found to appear through torus-doubling bifurcations, in contrast to the case of the coupled logistic map without torus doublings. With decreasing b, we have investigated the mechanisms for the disappearance of torus doublings and have found that doubled tori are replaced with simple tori, periodic attractors, or chaotic attractors for small b. Similar torus doublings is also found in two symmetrically coupled pendula that individually display a period-doubling route to chaos. Finally, these torus doublings are expected to be observed in real experiments of coupled period-doubling systems, such as two resistively coupled p-n junction resonators [24] and two inductively coupled electronic frequency generators [25].

REFERENCES

[1] E. Ott, *Chaos in Dynamical Systems* (Cambridge University Press, New York, 2002), p. 212.
[2] S. J. Shenker, Physica D **5**, 405 (1982); M. J. Feigenbaum, L. P. Kadanoff and S. J. Shenker, Physica D **5**, 370 (1982); D. Rand, O. Ostlund, J. Sethna and E. Siggia, Phys. Rev. Lett. **49**, 132 (1982).
[3] M. H. Jensen, P. Bak and T. Bohr, Phys. Rev. A **30**, 1960 (1984).

[4] K. Kaneko, Prog. Theor. Phys. **69**, 1806 (1983); *ibid.* **72**, 202 (1984).
[5] M. J. Feigenbaum, J. Stat. Phys. **19**, 25 (1978); *ibid.* **21**, 669 (1979).
[6] A. Arnéodo, P. H. Coullet and E. A. Spiegel, Phys. Lett. A **94**, 1 (1983).
[7] V. Franceschini, Physic D **6**, 285 (1983).
[8] J.-I. Kim, H.-K. Park and H.-T. Moon, Phys. Rev. E **55**, 3948 (1997).
[9] M. Sano and Y. Sawada, *Chaos in Statistical Methods* (Springer-Verlag, Berlin, 1984), p. 226.
[10] J.-M. Flesselles, V. Croquette and S. Jucquois, Phys. Rev. Lett. **72**, 2871 (1994).
[11] K. E. McKell, D. S. Broomhead, R. Jones and D. T. J. Hurle, Europhys. Lett. **12**, 513 (1990).
[12] M. R. Bassett and J. L. Hudson, Physica D **35**, 289 (1989).
[13] J. C. Shin and S.-I. Kwun, Phys. Rev. Lett. **82**, 1851 (1999); J. C. Shin. Phys. Rev. E **60**, 5394 (1999).
[14] M. Diestelhorst, K. Barz, H. Beige, M. Alexe and D. Hesse, Phil. Trans. R Soc. A **366**, 437 (2008).
[15] M. Hénon, Q. Appl. Math. **27**, 291 (1969); *ibid.* Commun. Math. Phys. **50**, 69 (1976).
[16] S. Kuznetsov, Radiophys. Quantum Electron. **28**, 681 (1985); E. N. Erastova and S. P. Kuznetsov, Sov. Phys. Tech. Phys. **36**, 130 (1991).
[17] H. Kook, F. H. Ling and G. Schmidt, Phys. Rev. A **43**, 2700 (1991).
[18] C. Reick and E. Mosekilde, Phys. Rev. E **52**, 1418 (1995).
[19] A. J. Lichtenberg and M. A. Liberman, *Regular and Stochastic Motion* (Springer-Verlag, New York, 1983), p. 283.
[20] K. Geist and W. Lauterborn, Physica D **41**, 1 (1990).
[21] S.-Y. Kim and K. Lee, Phys. Rev. E **54**, 1237 (1996).
[22] S.-Y. Kim and K. Lee, Phys. Rev. E **53**, 1579 (1996).
[23] S. Lefschetz, *Differential Equations: Geometric Theory* (Dover Publications, New York, 1977), Sec. 3.5.
[24] R. Van Buskirk and C. Jeffries, Phys. Rev. A **31**, 3332 (1985).
[25] V. S. Anishchenko, *Dynamical Chaos in Physical Systems* (Teubner, Leipzig, 1989).